Mechanics of Time-Dependent Materials (2023) 27:251–274
https://doi.org/10.1007/s11043-023-09609-9

RESEARCH

An accelerated creep model for the rock downstream of a Xianglushan tunnel

Wenbo Liu[1,2] · Qing Liu[3] · Jian Li[3] · Hui Zhou[1,2] · Chengwei Zhao[1,2] · Yong Yang[4]

Received: 12 April 2023 / Accepted: 30 May 2023 / Published online: 14 June 2023

Abstract
Rheological characterization of the rock surrounding the lower wall of Xianglushan No. 2 tunnel was made to investigate the degree of stability for assurance of the long-term stability of the rock. The creep parameters were extracted for the creep model for the rock mass in the fault zone. A micro-element was introduced to describe the accelerated creep deformation and a new accelerated creep model was established. The creep parameters were extracted by allowing the creep modeling results to fit feature points in the creep curves under different creep loads. The role of various creep parameters on creep behavior was identified. The results showed that the creep modeling results agreed with the experimental data, validating the creep model and the associated parameter determination method.

Keywords Triaxial creep · Time · Damage creep model · Method for determining creep parameters

1 Introduction

As shallow mineral resources are scarce, attention is turning to the second depth space for mining. The deep rock mass is usually in an environment of high in-situ stress, high temperature, and high seepage field. The mechanical properties of rock and the geotechnical materials under a low-stress state show different mechanical strength characteristics (Aditya et al. 2018; Cornet and Dabrowski 2018; Wang et al. 2018a). Not only does the deep surrounding rock have obvious rheological properties, but also, such hard rock as granite has a rheological effect. Under a low confining pressure, it generally obeys the strength criterion of linear geomaterials, and under a high confining pressure, it has obvious nonlinear characteristics (Jing et al. 2018; Riva et al. 2018; Tomanovic 2016). With the increase of confining pressure, the failure state of rock changes from brittle failure to ductile failure (Wu et al.

✉ J. Li
plmojn2022@163.com

1 State Key Laboratory of Geomechanics and Geotechnical Engineering, Institute of Rock and Soil Mechanics, Chinese Academy of Sciences, Wuhan, Hubei 430071, China

2 University of Chinese Academy of Sciences, Beijing 100049, China

3 Yunnan Dian Zhong Water Diversion Engineering Co., Ltd., Kunming 650000, China

4 China Railway 11th Bureau Group City Rail Engineering Co., Ltd, Wuhan 430074, China

2015). The mechanical strength and creep parameters of deep surrounding rock decrease with the deterioration of geological conditions. (Andargoli et al. 2018; Huang and Liu 2011; Liu and Li 2018).

Rheological tests are carried out under the corresponding geological environment to study the rheological properties of rocks (Jin and Cristescu 1998; Li et al. 2017). To analyze the stability of underground structures under long-term stress, rock indoor creep tests were conducted under different influencing factors, and the influence degrees of various factors on creep deformation were analyzed (Eslami et al. 2018). The creep behavior and damage evolution characteristics of salt rock under long-term cycles and constant loads under different stress levels are analyzed. It is helpful to lay a foundation for the research of structural stability of underground waste disposal. (Wang et al. 2018b). At the same time, using the triaxial creep test data to study the rock-water coupling creep characteristics is necessary. The creep behavior of sandstone under different permeability is analyzed (Xu et al. 2018a). Xu et al. (2018b) propose a method for determining rock creep parameters. This method only considers the effect of the stress state on creep parameters. However, the creep parameters are also affected by time, osmotic pressure, and other factors (Hamza and Stace 2018; Qi et al. 2012; Yoshida and Horii 1992; Zhou et al. 2010). However, the model uses software and least squares to determine the parameters, not a clear method to determine the parameters (Hao et al. 2017; Ma et al. 2017; Singh et al. 2018). Therefore, a creep determination method is proposed to analyze the relationship between creep parameters and stress and time. A creep model considering the time-dependent creep parameters is obtained by substituting the above equations into the creep model. Finally, it is necessary to compare the model and test curves. The correctness and rationality of the method are verified by the coincidence degree between the two methods.

2 Determination of rock creep parameters

2.1 Improved creep model

The improved creep model is shown in Fig. 1 (Hou et al. 2018).

The creep equation is

$$\varepsilon = \begin{cases} \dfrac{\sigma}{E_0} + \dfrac{\sigma}{E_1}\left[1 - \exp(-\dfrac{E_1}{\eta_1}t)\right] + \dfrac{\sigma}{\eta_2}t, & \sigma < \sigma_s, \\ \dfrac{\sigma}{E_0} + \dfrac{\sigma}{E_1}\left[1 - \exp(-\dfrac{E_1}{\eta_1}t)\right] + \dfrac{\sigma}{\eta_2}t + \dfrac{\sigma}{E_2(1-D)}, & \sigma \geq \sigma_s, \end{cases} \tag{1}$$

where E_0 is the elastic modulus, E_1 is the viscoelastic modulus, η_1 is the viscosity coefficient of the viscoelastic body, η_2 is the viscosity coefficient of the viscoplastic body, ε

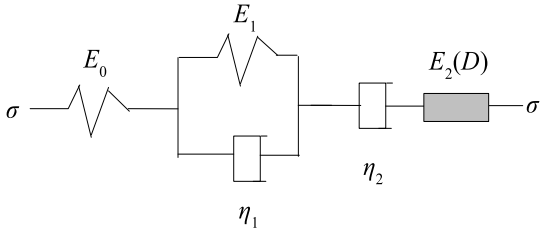

Fig. 1 The improved creep model

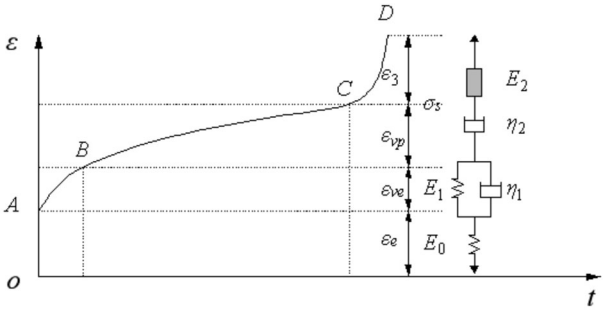

Fig. 2 Corresponding schematic diagram of the obtained model and the creep curve

is creep deformation, σ is the stress, t is the whole creep process time, E_2 is the elastic modulus of the viscoplastic body, and D is the damage variable.

The elastic strain ε_e, viscoelastic strain ε_{ve}, viscoplastic strain ε_{vp}, and strain ε_3 are

$$\begin{cases} \varepsilon_e = \dfrac{\sigma}{E_0}; \varepsilon_{ve} = \dfrac{\sigma}{E_1}\left[1 - \exp(-\dfrac{E_1}{\eta_1}t)\right], \\ \varepsilon_{vp} = \dfrac{\sigma}{\eta_2}t; \varepsilon_3 = \dfrac{\sigma}{E_2(1-D)}. \end{cases} \tag{2}$$

To make each part of the established model correspond to the classic creep decentering of the rock, the expression of each creep parameter can be derived from the characteristic points of the creep deformation curve. The components in the revised model correspond to the various stages of the classic rock deformation curve. The corresponding schematic diagram of the obtained model and the creep curve is shown in Fig. 2.

2.2 Creep equation of elastic modulus of the viscoplastic body

The Kachanov creep damage model is as follows.

$$\begin{cases} \dfrac{dD}{dt} = \left[\dfrac{\sigma}{A(1-D)}\right]^{N+2}, \\ A = \left(2ESK^N\right)^{1/(2+N)}, \end{cases} \tag{3}$$

where A, E, S, K, and N are material parameters.

After Equation (3) is integrated, the damage variable can be obtained as

$$D = 1 - \left[1 - \left(\frac{\sigma}{A}\right)^{N+2}(N+3)\left(t - t^*\right)\right]^{\frac{1}{N+3}}, \tag{4}$$

where t^* is the moment of accelerated creep of the rock.

$$\left(\frac{\sigma}{A}\right)^{N+2}(N+3) = \frac{1}{t_F - t^*}, \tag{5}$$

where t_F is the creep failure time.

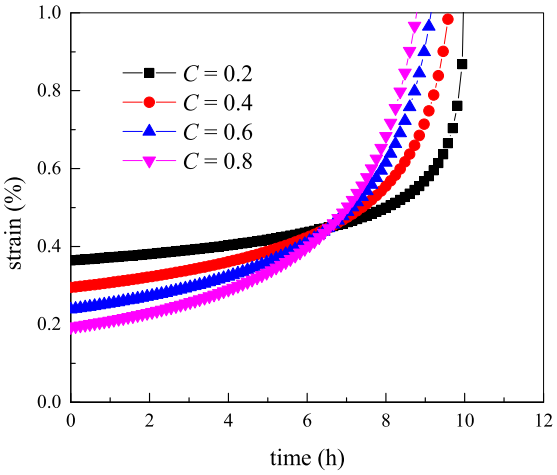

Fig. 3 Parameter sensitivity analysis of new components

The damage variable D is

$$D = 1 - \left(\frac{t_F - t}{t_F - t^*}\right)^{\frac{1}{N+3}} = 1 - \left(\frac{t_F - t}{t_F - t^*}\right)^{C}, \tag{6}$$

where C is the coefficient of damage.

Equation (6) is substituted into Equation (2), and the modified Burgers model creep equation is

$$\varepsilon = \begin{cases} \dfrac{\sigma}{E_0} + \dfrac{\sigma}{E_1}\left[1 - \exp(-\dfrac{E_1}{\eta_1}t)\right] + \dfrac{\sigma}{\eta_2}t, & \sigma < \sigma_s, \\ \dfrac{\sigma}{E_2}\left(\dfrac{t_F - t}{t_F - t^*}\right)^{-C} + \dfrac{\sigma}{E_0} + \dfrac{\sigma}{E_1}\left[1 - \exp(-\dfrac{E_1}{\eta_1}t)\right] + \dfrac{\sigma}{\eta_2}t, & \sigma \geq \sigma_s, \end{cases} \tag{7}$$

where σ_s is the long-term strength.

When $t \to t_F$ and creep deformation reaches accelerating creep deformation, the following $\varepsilon \to \infty$ and $d\varepsilon/dt \to \infty$ relations are satisfied.

The parameter sensitivity analysis of the components introduced to describe the accelerated creep deformation is carried out. When $t_F = 10.07$ h, $t^* = 6.58$ h, $\sigma = 90$ MPa, and $E_2 = 200$ GPa · h, the influence of damage influence coefficient C on the creep curve is analyzed.

It can be seen from Fig. 3 that the larger the damage influence coefficient C, the less steep the creep curve and the shorter the creep time. That is, rock is more prone to creep deformation and failure. At the same time, the strain value at the starting point of accelerated creep is smaller. The degree of agreement for describing the accelerated creep deformation law will also decrease.

2.3 Three-dimensional creep constitutive model

The transformation condition of the three-dimensional model is (Ma et al. 2013).

$$\begin{cases} \sigma_{ij} = S_{ij} + \delta_{ij}\sigma_m, S_{ij} = 2G_1 e_{ij}, \\ \varepsilon_{ij} = e_{ij} + \delta_{ij}\varepsilon_m, \sigma_m = 3K\varepsilon_m, \end{cases} \tag{8}$$

where δ_{ij} is the Kronecker function, G_1 is the shear modulus, K is the bulk modulus, σ_m is the stress sphere tensor, S_{ij} is the stress deviatoric tensor, and ε_m is the strain sphere tensor, $\sigma_m = (\sigma_1 + 2\sigma_3)/3$, $\varepsilon_m = (\varepsilon_1 + 2\varepsilon_3)/3$, $S_{ij} = \sigma_{ij} - \sigma_m$.

When $\sigma < \sigma_s$,

$$\varepsilon_{11} = \frac{\sigma_1 - \sigma_3}{3G_0} + \frac{\sigma_1 + 2\sigma_3}{9K_0} + \frac{\sigma_1 - \sigma_3}{3G_1}\left[1 - \exp\left(-\frac{G_1}{\eta_1}t\right)\right] + \frac{\sigma_1 - \sigma_3}{3\eta_2}t, \tag{9}$$

where G_2 is the shear modulus of the viscoelastic body.

When $\sigma \geq \sigma_s$,

$$\begin{aligned}\varepsilon_{11} = &\frac{\sigma_1 - \sigma_3}{3G_0} + \frac{\sigma_1 + 2\sigma_3}{9K_0} + \frac{\sigma_1 - \sigma_3}{3G_1}\left[1 - \exp\left(-\frac{G_1}{\eta_1}t\right)\right] \\ &+ \frac{\sigma_1 - \sigma_3}{3\eta_2}t + \frac{\sigma_1 - \sigma_3}{3G_2}\left(\frac{t_F - t}{t_F - t^*}\right)^{-C}.\end{aligned} \tag{10}$$

3 Creep model parameter determination

The time t_F and time t^* of rock can be calculated by experiments (Zhou et al. 2011). Rock shear modulus G_0 and bulk modulus K_0 satisfy Equation (11) and are calculated as follows.

$$K_0 = \frac{\sigma_m}{3\varepsilon_m} = \frac{\sigma_m}{\varepsilon_v};\ G_0 = \frac{3K_0 S_{ij}}{2\left(3K_0\varepsilon_0 - \sigma_m\right)}, \tag{11}$$

where ε_v is the volume strain.

Because the shear modulus G_0 of the rock is only affected by the stress state, the parameter determination under the action of time t is not discussed. However, the bulk modulus K_0 is indeed affected by the time t. The value of the bulk modulus K_0 at various times can be obtained by combining Equation (11) and the test data.

When the creep of the tunnel surrounding rock changes to steady creep, the creep value can be the sum of decay creep and transient strain.

$$\begin{aligned}&\lim_{t\to\infty}\left[\frac{\sigma_1 - \sigma_3}{3G_0} + \frac{\sigma_1 + 2\sigma_3}{9K_0} + \frac{\sigma_1 - \sigma_3}{3G_1}\left[1 - \exp\left(-\frac{G_1}{\eta_1}t\right)\right]\right] \\ &= \frac{\sigma_1 - \sigma_3}{3G_0} + \frac{\sigma_1 + 2\sigma_3}{9K_0} + \frac{\sigma_1 - \sigma_3}{3G_{1\infty}},\end{aligned} \tag{12}$$

where $G_{1\infty}$ is the viscoelastic modulus when $t \to \infty$.

The following relation exists at any time t_i on the stable creep deformation curve.

$$\varepsilon_{11i}^{eve} = \frac{\sigma_1 - \sigma_3}{3G_0} + \frac{\sigma_1 + 2\sigma_3}{9K_{0i}} + \frac{\sigma_1 - \sigma_3}{3G_{1\infty}} + \frac{\sigma_1 - \sigma_3}{3\eta_{2i}}t_i. \tag{13}$$

If another time t_j is arbitrarily taken near time t_i, the parameter value is considered to be stable and unchanged in this interval.

$$\varepsilon_{11j}^{eve} = \frac{\sigma_1 - \sigma_3}{3G_0} + \frac{\sigma_1 + 2\sigma_3}{9K_{0j}} + \frac{\sigma_1 - \sigma_3}{3G_{1\infty}} + \frac{\sigma_1 - \sigma_3}{3\eta_{2j}}t_j. \tag{14}$$

The η_{2i} at any time is

$$\eta_{2i} = \frac{\left(t_i - t_j\right)\left(\sigma_1 - \sigma_3\right)}{3\left(\varepsilon_{11i}^{eve} - \varepsilon_{11j}^{eve}\right)}. \tag{15}$$

When $\sigma < \sigma_s$, a time point t_i on the creep curve is arbitrarily taken. Then, there is the following relationship.

$$\varepsilon_{11i} = \frac{\sigma_1 - \sigma_3}{3G_0} + \frac{\sigma_1 + 2\sigma_3}{9K_{0i}} + \frac{\sigma_1 - \sigma_3}{3G_{1i}}\left[1 - \exp\left(-\frac{G_1}{\eta_1}t_i\right)\right] + \frac{\sigma_1 - \sigma_3}{3\eta_{2i}}t_i. \tag{16}$$

By performing the first derivative of time t for Equation (9), an arbitrary time point, t_i is taken on the creep curve to obtain Equation (17).

$$\varepsilon'_{11i} = \frac{\sigma_1 - \sigma_3}{3\eta_{1i}}\exp\left(-\frac{G_{1i}}{\eta_{1i}}t_i\right) + \frac{\sigma_1 - \sigma_3}{3\eta_{2i}}. \tag{17}$$

For the convenience of calculation, the Taylor formula expansion is performed on the exponential function in Equation (17).

$$\exp\left(-\frac{G_{1i}}{\eta_{1i}}t_i\right) = 1 - \frac{G_{1i}}{\eta_{1i}}t_i + o\left(t_i^2\right). \tag{18}$$

Equation (18) is substituted into Equations (16) and (17) to obtain Equations (19) and (20).

$$\varepsilon'_{11i} = \frac{\sigma_1 - \sigma_3}{3\eta_{1i}}\left(1 - \frac{G_{1i}}{\eta_{1i}}t_i\right) + \frac{\sigma_1 - \sigma_3}{3\eta_{2i}}, \tag{19}$$

$$\varepsilon_{11i} = \frac{\sigma_1 - \sigma_3}{3G_0} + \frac{\sigma_1 + 2\sigma_3}{9K_{0i}} + \frac{\sigma_1 - \sigma_3}{3G_{1i}}\left(1 - \frac{G_{1i}}{\eta_{1i}}t_i\right) + \frac{\sigma_1 - \sigma_3}{3\eta_{2i}}t_i. \tag{20}$$

The shear modulus G_{1i} and viscosity coefficient η_{1i} under the action of different times are

$$G_{1i} = \frac{\eta_{1i}}{t_i}\left[1 - \left(\varepsilon'_{11i} - \frac{\sigma_1 - \sigma_3}{3\eta_{2i}}\right)\frac{3\eta_{1i}}{\sigma_1 - \sigma_3}\right], \tag{21}$$

$$\eta_{1i} = \frac{\left(\sigma_1 - \sigma_3\right)}{\left(\varepsilon'_{11i} - \frac{\sigma_1 - \sigma_3}{3\eta_{2i}}\right)} - \frac{\left(\sigma_1 - \sigma_3\right)t_i}{\left(\varepsilon_{11i} - \frac{\sigma_1 - \sigma_3}{3G_0} - \frac{\sigma_1 + 2\sigma_3}{9K_{0i}} - \frac{\sigma_1 - \sigma_3}{3\eta_{2i}}t_i\right)}. \tag{22}$$

When $\sigma \geq \sigma_s$, the first derivative of time t is carried out to Equation (10). A time point t_i can be arbitrarily taken on the creep curve to obtain Equation (23).

$$\varepsilon'_{11i} = \frac{\sigma_1 - \sigma_3}{3\eta_{1i}}\left(1 - \frac{G_{1i}}{\eta_{1i}}t_i\right) + \frac{\sigma_1 - \sigma_3}{3\eta_{2i}} + \frac{C_i}{t_F - t^*}\frac{\sigma_1 - \sigma_3}{3G_{2i}}\left(\frac{t_F - t_i}{t_F - t^*}\right)^{-C_i - 1}. \tag{23}$$

The ε_{11i} is

$$\varepsilon_{11i} = \frac{\sigma_1 - \sigma_3}{3G_0} + \frac{\sigma_1 + 2\sigma_3}{9K_{0i}} + \frac{\sigma_1 - \sigma_3}{3G_{1i}}\left[1 - \exp\left(-\frac{G_{1i}}{\eta_{1i}}t_i\right)\right] + \frac{\sigma_1 - \sigma_3}{3\eta_{2i}}t_i + \frac{\sigma_1 - \sigma_3}{3G_{2i}}\left(\frac{t_F - t_i}{t_F - t^*}\right)^{-C_i}. \tag{24}$$

The damage degree influence coefficient C_i and the shear modulus G_{2i} are

$$C_i = \frac{\left[\varepsilon'_{11i} - \frac{\sigma_1-\sigma_3}{3\eta_{1i}}\left(1-\frac{G_{1i}}{\eta_{1i}}t_i\right) - \frac{\sigma_1-\sigma_3}{3\eta_{2i}}\right](t_F - t_i)}{\varepsilon_{11i} - \frac{\sigma_1-\sigma_3}{3G_0} - \frac{\sigma_1+2\sigma_3}{9K_{0i}} - \frac{\sigma_1-\sigma_3}{3G_{1i}}\left[1-\exp\left(-\frac{G_{1i}}{\eta_{1i}}t_i\right)\right] - \frac{\sigma_1-\sigma_3}{3\eta_{2i}}t_i}, \tag{25}$$

$$\frac{1}{G_{2i}} = \left\{\varepsilon_{11i} - \frac{\sigma_1-\sigma_3}{3G_0} - \frac{\sigma_1+2\sigma_3}{9K_{0i}} - \frac{\sigma_1-\sigma_3}{3G_{1i}}\left[1-\exp\left(-\frac{G_{1i}}{\eta_{1i}}t_i\right)\right] - \frac{\sigma_1-\sigma_3}{3\eta_{2i}}t_i\right\} \times \left(\frac{t_F-t_i}{t_F-t^*}\right)^{C_i}\frac{3}{(\sigma_1-\sigma_3)}. \tag{26}$$

The above process is the method to determine the creep parameters.

4 Indoor creep test

4.1 Indoor triaxial compression test

The test object in this study is the surrounding rock of the No. 2 tunnel in the Dali Section 1 of the Central Yunnan Water Diversion Project. According to the standards and requirements of the International Society of Rock Mechanics, the rock samples are processed into cylinders with a height of 100 mm and a radius of 25 mm. The flatness of the upper and lower ends of the rock is less than 0.05 mm. The errors in height and diameter are within 0.3 mm. After removing the rock samples with obviously visible cracks, the wave velocity of rock samples is measured by an ultrasonic detection system. The rock samples with similar wave velocities are classified as a class for testing. It can ensure the authenticity and reliability of the test data. The physical size of the rock sample is measured by an electronic scale with an accuracy of 0.1 g and a standard vernier caliper. The physical size of the rock sample is obtained, as shown in Table 1. To make the measurement data accurate, three positions are selected for separate measurements in the measurement process of height and diameter. The average of the three data is taken as the actual measurement value.

The sample is shown in Fig. 4(a). The test equipment is a real-time high-temperature conventional triaxial test system independently developed by the Institute of Rock and Soil Mechanics, Chinese Academy of Sciences (Fig. 4(b)). The equipment can realize the nonlinear multi-field coupling test of the whole process of rock pore and fracture seepage in a deep, complex environment such as high temperature, high stress, high water pressure, and chemical corrosion.

The specific test steps are as follows.

(1) To prevent the sudden brittle failure of rock, it is necessary to set the upper limit of displacement before applying axial stress.

(2) The confining pressure is applied to the predetermined value at the oil loading rate of 1 ml / min. During the test, the confining pressure needs to be kept unchanged.

(3) Axial stress is applied at a loading rate of 1 ml / min. When the rock reaches the peak strength failure, the axial displacement of the same rate is continued until the residual strain of the rock is measured.

(4) The measured data were stored at intervals of 5 s.

(5) It is necessary to unload the confining pressure first and then unload the axial stress.

Table 1 Physical parameters of rock

Rock specimen	Height (mm)	Diameter (mm)	the ratio of height to diameter	Quality (g)	Saturation density (g/cm^{-3})
A1	99.79	49.95	2.00	491.7	2.501
A2	100.22	49.95	2.01	493.3	2.497
A3	100.11	50.20	1.99	492.2	2.470
A4	100.28	50.15	2.00	492.4	2.472
A5	100.18	50.07	2.00	495.4	2.462
B1	100.06	49.99	2.00	494.2	2.503
B2	99.91	50.07	2.00	492.4	2.489
B3	101.03	49.93	2.02	497.9	2.503
B4	100.61	49.97	2.01	497.0	2.505
C1	101.02	50.03	2.02	504.5	2.525
C2	101.05	50.00	2.02	503.5	2.525
C3	100.83	50.21	2.01	504.5	2.515
C4	100.42	49.91	2.01	516.2	2.615

Fig. 4 Rock sample

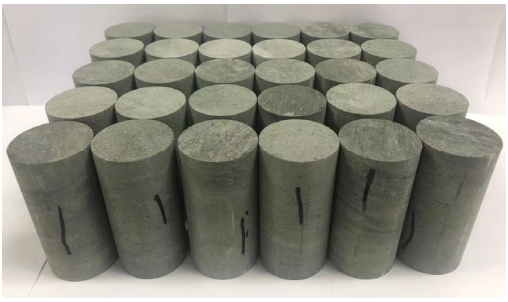

(a)Rock sample

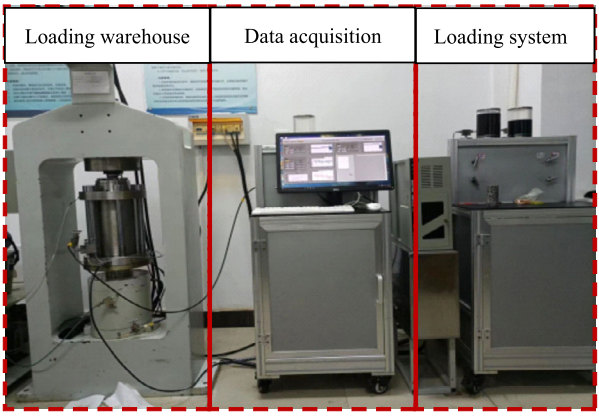

(b) Physical map of the rock test system

Fig. 5 Stress-strain curve

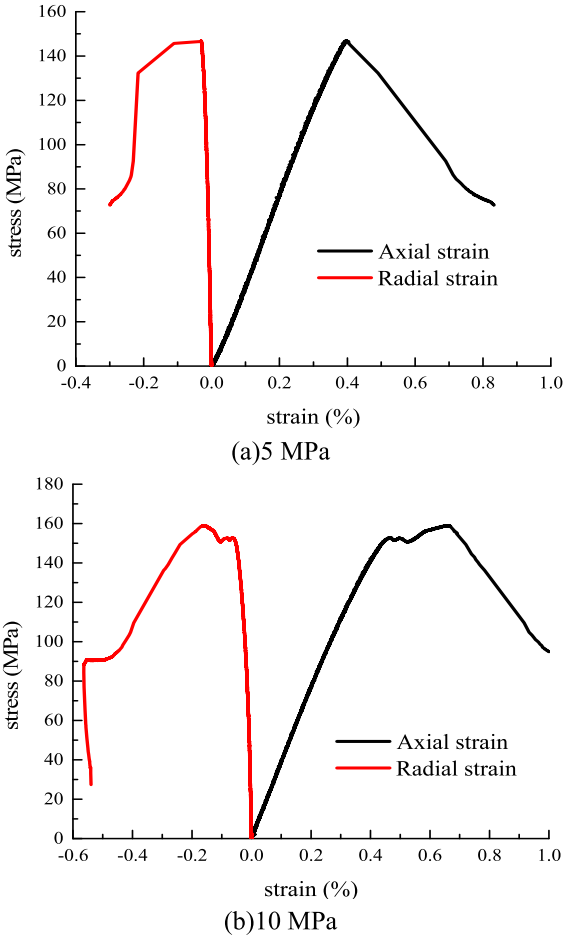

(6) After the hydraulic oil in the cabin is extracted, the damaged rock samples are taken out, marked, and stored.

The confining pressures are set at 5 MPa, 10 MPa, 15 MPa, 20 MPa, and 25 MPa, respectively (Munson et al. 1993). Figure 5 shows the stress-strain curve of rocks under different confining pressures.

According to Fig. 5, the variation of rock under different confining pressures is similar. In the pre-peak deformation stage, the stress of the rock increases with the increase of strain until the peak strength. In the post-peak deformation stage, the stress of the rock decreases with the increase of strain until the residual strength. In the residual deformation stage, rock stress shows a constant trend with the increase of strain. At the same time, the peak strength of rock increases with the increase of confining pressure. This is due to the restriction of confining pressure on the circumferential deformation during the loading process, which improves the bearing capacity of the rock.

The number of cracks formed on the surface of the specimen after failure under low confining pressure is less than that under high confining pressure. This is because the confining pressure has a certain reinforcing effect on the rock. When the confining pressure is low, the main crack propagation speed is relatively fast. After the main crack is penetrated, the

Fig. 5 (*Continued*)

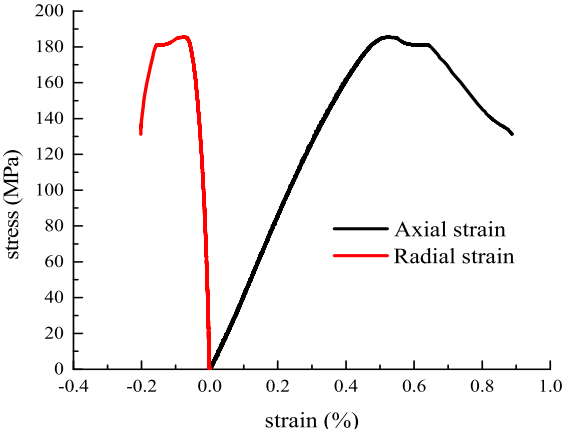

(c)15 MPa

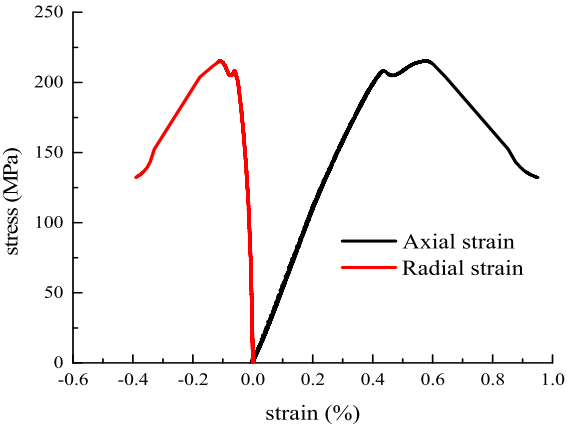

(d)20 MPa

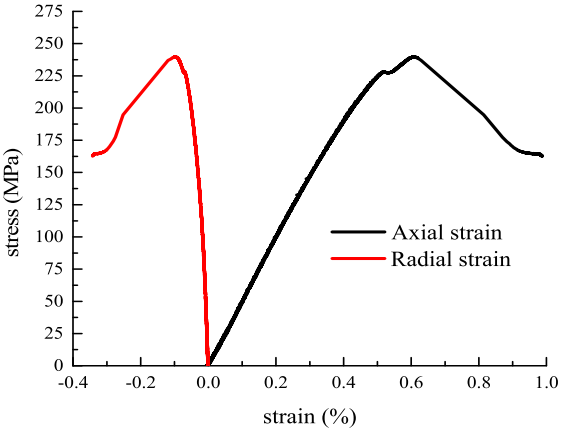

(e)25 MPa

specimen is destroyed immediately after forming the fracture surface. When the confining pressure is high, the existence of high confining pressure inhibits the development speed of the main crack. The airfoil crack near the main crack develops and expands. Finally, these microscopic crack propagation intersections form microscopic cracks on the rock surface. Therefore, there are more cracks on the rock surface under high confining pressure than under low confining pressure.

4.2 Creep test plan

In the triaxial rheological test, it is necessary to apply confining pressure to a predetermined value. After the deformation of the first level of the stress level is stabilized, the axial load is applied to a predetermined value and remains constant. The axial strain and time relationship of rock samples need to be measured and recorded. According to the experimental scheme, axial compression loading is carried out step by step, and the confining pressure must be kept constant during the loading process. When the rock creeps into a stable creep phase or the deformation is stable, the loading of the next-stage axial pressure can be performed. According to the above steps, the axial load is applied until the rock is unstable.

4.3 Analysis of axial creep results

The specific experimental scheme of triaxial creep is as follows.

(1) The initial stress level is 60% of the peak strength of the triaxial test rock.

(2) To facilitate the application of stress, the initial value of stress is an integer. The stress levels of the samples with confining pressure of 10 MPa are divided into 100 MPa, 110 MPa, 120 MPa, 130 MPa, and 140 MPa.

(3) The confining pressure is applied to the predetermined value at the oil loading rate of 1 ml / min. When the surrounding rock is stable, the axial stress is applied. Moreover, it is necessary to keep the confining pressure unchanged throughout the test.

(4) The axial stress is applied to the predetermined value at the oil loading rate of 1 ml / min. After the first-stage load deformation is stable, the next-stage load is applied until the specimen is deformed and destroyed.

(5) After the test is completed, the confining pressure is unloaded to zero, and the axial pressure is unloaded to zero. The hydraulic oil in the pressure chamber is pumped back into the equipment, and the pressure chamber is lifted to remove the rock sample for preservation. The test data storage interval is 5 s, and the final test data can be exported.

The axial deformation history curve is shown in Fig. 6.

From Fig. 6, it can be seen that the proportion of creep deformation to total deformation decreases first and then increases. Furthermore, creep deformation accounts for more and more total deformation. It shows that the internal pores of the rock continue to develop, which leads to the more obvious deterioration characteristics of the rock. However, comparing and analyzing the instantaneous strain and creep strain shows that the proportion of instantaneous strain to total deformation is far greater than that of creep strain to total deformation. It shows that the damage caused by instantaneous strain to rock is greater than that caused by creep to rock. Taking the confining pressure of 25 MPa as an example, when the stress is 200 MPa, the creep rate of the rock decays to zero after a long time. The total creep time is about 47.80 h. When the stress is 220 MPa, the rock has an obvious accelerated creep stage. The accelerated creep time decreases with the increase in stress level, and the total creep time is about 20.61 h. It shows that the increase in stress aggravates the damage development and fracture expansion inside the rock, making it more prone to damage. When

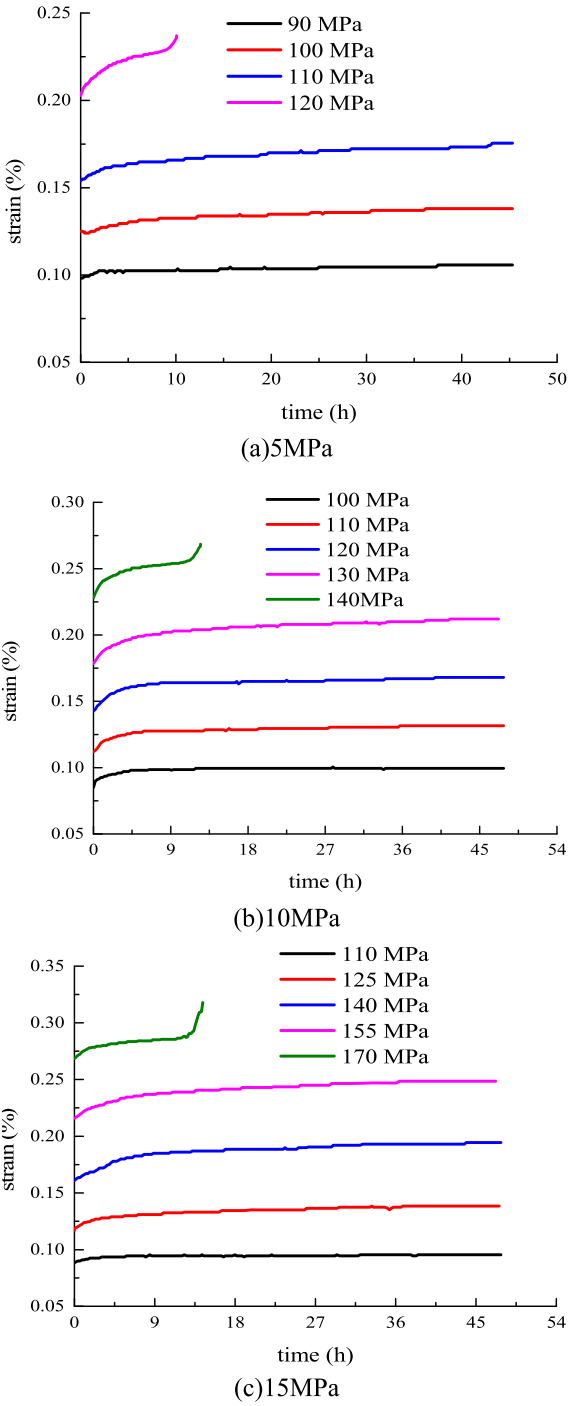

Fig. 6 Axial creep curves at all levels of stress

Fig. 6 (*Continued*)

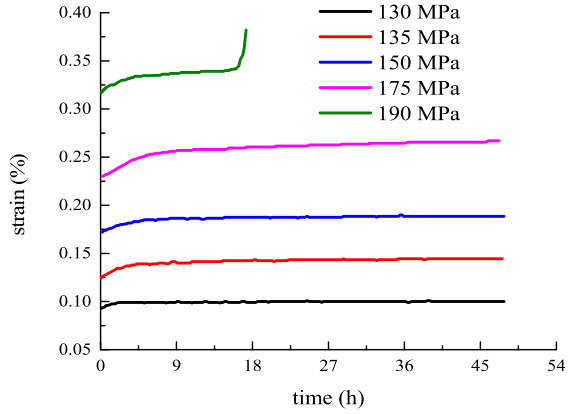

(d)20MPa

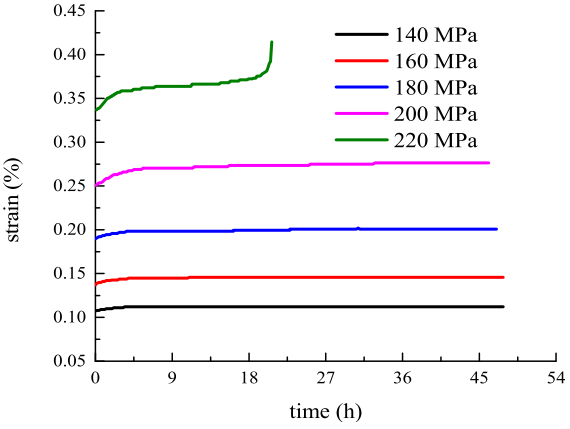

(e)25MPa

the confining pressure is 20 MPa, the creep deformation time under failure stress is 17.21 h. When the confining pressure is 25 MPa, the creep deformation time under the action of failure stress is 20.61 h. This shows that the increase of confining pressure can effectively improve the bearing capacity of the rock, the creep failure time of the rock, and the time of the accelerated creep stage.

4.4 Creep rate

The creep rate of rock under a confining pressure of 5 MPa is shown in Fig. 7.

It can be seen from Fig. 7 that under low stress, as time increases, the creep rate value begins to decrease until it decays to zero. At this time, the deformation value of the creep curve under a low-stress level is close to the coordinate axis of axial deformation. Under the action of medium stress, the rock has a large creep rate value at the initial loading time. However, the creep rate is much smaller than the initial creep rate under the first load. As time increases, the creep rate value begins to decrease, and the creep rate will decay to a stable value. Under failure stress, the material also has a large creep rate value at the initial

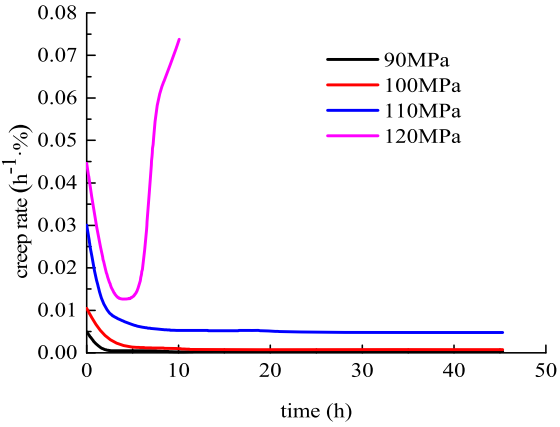

Fig. 7 Creep rate

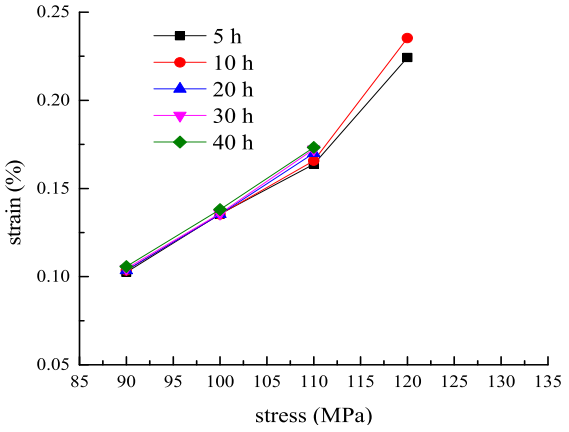

Fig. 8 Isochronous stress-strain curve

loading time. With the increase of time, the creep rate value first decays to a stable value and then increases rapidly until the creep instability failure of the material occurs. The creep rate after the final failure is much larger than the initial creep rate.

4.5 Isochronous stress-strain curve

As can be seen from Fig. 8, σ_s of 5 MPa confining pressure is 100 MPa (Liu and Zhang 2020a).

Figure 8 shows that the variation of rock strain at the divergence point and before is very small under the same stress level. This is shown in the figure concentrated on one point. Moreover, the stress and strain before the divergence point are linear. However, after the divergence point, as the stress increases, the rock strain changes more and more under the same stress level. Moreover, there is a nonlinear trend between stress and general. In general, the stress value corresponding to the divergence point is taken as the long-term strength value of the rock.

5 Creep parameter variation law and model establishment

From a conceptual point of view, the viscosity coefficient η is equal to the stress σ divided by the strain rate $d\varepsilon/dt$. Because there is a time t, the viscosity coefficient η is considered a variable. However, the nonlinearity of creep should not only be reflected in the change of one parameter of the viscosity coefficient — all creep parameters should be regarded as variables. The nonlinear characteristics of rock creep come from the change in the microscopic level inside the rock. The reasons for the change include stress, time, and external conditions (seepage, temperature, chemical factors, etc.). In practical engineering, rock mechanical parameters vary with stress and time. Many studies have proved that the creep parameters of rocks usually decrease with time. The model parameters are shown in Table 2.

The relation curve of the creep parameter and time can be drawn, as shown in Fig. 9. The relationship between other creep parameters and time can be described using an exponential

Table 2 Creep parameters at different times (5 MPa)

Parameter	Stress (MPa)	Time (h)							
		2	4	6	8	10	20	30	40
G_0 (GPa)	90	7.840	7.840	7.840	7.840	7.840	7.840	7.840	7.840
	100	4.881	4.881	4.881	4.881	4.881	4.881	4.881	4.881
	110	3.706	3.706	3.706	3.706	3.706	3.706	3.706	3.706
	120	3.008	3.008	–	–	–	–	–	–
K_0 (GPa)	90	170.819	189.367	206.327	227.726	257.896	289.361	313.008	330.541
	100	163.973	179.317	208.460	279.142	−285.408	−253.629	−219.496	−198.653
	110	−586.972	−533.345	−493.464	−449.783	−428.478	−402.178	−385.517	−365.221
	120	−296.304	−293.968	−288.874	−286.166	−283.446	–	–	
G_1 (GPa)	90	42.595	41.865	40.273	39.427	38.577	37.254	36.17	35.640
	100	46.184	44.687	42.035	40.795	38.865	38.632	37.801	37.122
	110	48.922	45.987	43.245	41.642	39.875	40.324	39.166	38.151
	120	49.144	47.823	45.012	43.474	41.653	–	–	–
η_1 (GPa·h)	90	2474.7	2532.743	2618.442	2705.9719	2767.719	2889.519	2974.828	3000.012
	100	2242.693	2265.398	2365.807	2435.216	2532.084	2653.321	2800.111	2823.425
	110	2160.943	2192.505	2284.718	2366.101	2416.744	2549.648	2662.874	2710.124
	120	2201.589	2291.496	2377.868	2444.979	2465.676	–	–	
η_2 (GPa·h)	90	929.960	1248.507	1575.729	1898.474	2217.817	2478.268	2645.820	2698.014
	100	776.743	1010.617	1359.199	1534.679	1822.134	2180.159	2425.256	2500.142
	110	721.666	877.240	1135.037	1283.344	1342.070	1583.942	1768.082	1821.354
	120	603.517	828.810	1003.159	1158.778	1191.772	–	–	–
G_2 (GPa)	90	–	–	–	–	–	–	–	–
	100	641.437	553.708	495.080	383.255	401.144	285.155	165.414	154.344
	110	493.383	409.795	317.668	302.838	200.017	100.636	89.654	80.321
	120	254.181	228.657	207.896	196.324	188.432	–	–	–
C	90	–	–	–	–	–	–	–	–
	100	0.344	0.324	0.306	0.288	0.273	0.275	0.272	0.269
	110	0.327	0.315	0.280	0.263	0.268	0.266	0.258	0.257
	120	0.322	0.312	0.276	0.240	0.266	–	–	–

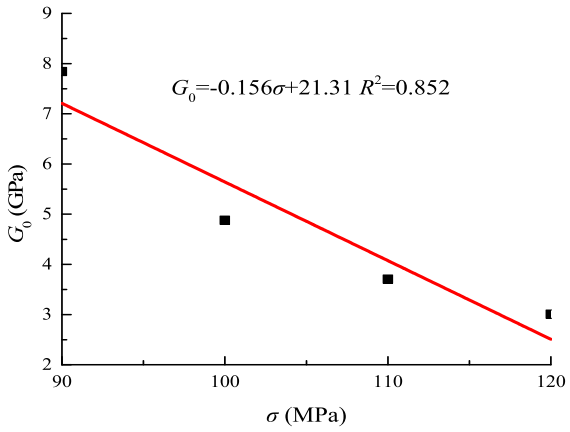

Fig. 9 Creep parameters and the time

(a) G_0

function (Liu and Zhang 2020b).

$$Z = a_i * \exp(-t/b_i) + c_i, \tag{27}$$

where a_i, b_i, and c_i are fitting parameters, and Z represents the creep parameters of the rock.

When the axial pressure is 100 MPa, the bulk modulus changes from positive to negative. The volume changes from compression state to expansion state. The instantaneous shear modulus decreases with the increase in stress. With the increase of time, the shear moduli G_1 and G_2 first decrease and then tend to be stable. As time goes on, the damage Influence coefficient C decreases continuously. This indicates that the damage degree of the rock is gradually increasing. As time goes on, the viscosity coefficient η_1 increases at first increases and then tends to be stable. This indicates that the creep deformation of the rock sample has entered the stage of stable creep. As time passes, the change law of viscosity coefficient η_2 is consistent with that of viscosity coefficient η_1.

In summary, the relationship between creep model parameters and time is obtained. The model parameters describing instantaneous, viscoelastic, and viscoplastic strain are basic. Only the parameters describing accelerated creep greatly influence the agreement between the final model and test curves. An accelerated creep deformation rate is increasing. When the rock creep deformation failure occurs, its accelerated creep deformation is suddenly increased. When the stress is 100 MPa and 110 MPa, the change law of damage influence coefficient C shows a trend of decreasing first and then stabilizing. However, when the stress is 120 MPa, the change law of damage influence coefficient C shows a decreasing trend, and the change range is relatively large. Therefore, when the damage influence coefficient C changes, its large change will affect the overall trend of the curve.

The fitting value of the above relation is shown in Table 3.

In summary, a modified creep model can be obtained.

When $\sigma < \sigma_s$,

$$\varepsilon_{11} = \frac{\sigma_1 - \sigma_3}{3G_0(\sigma)} + \frac{\sigma_1 + 2\sigma_3}{9K_0(t)} + \frac{\sigma_1 - \sigma_3}{3G_1(t)}\left[1 - \exp\left(-\frac{G_1(t)}{\eta_1(t)}t\right)\right] + \frac{\sigma_1 - \sigma_3}{3\eta_2(t)}t. \tag{28}$$

Fig. 9 (*Continued*)

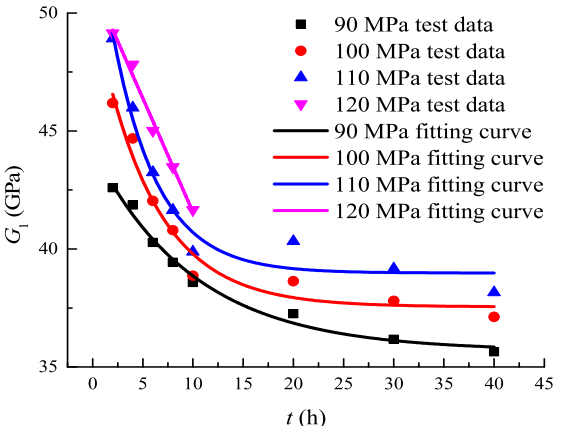

(b) G_1

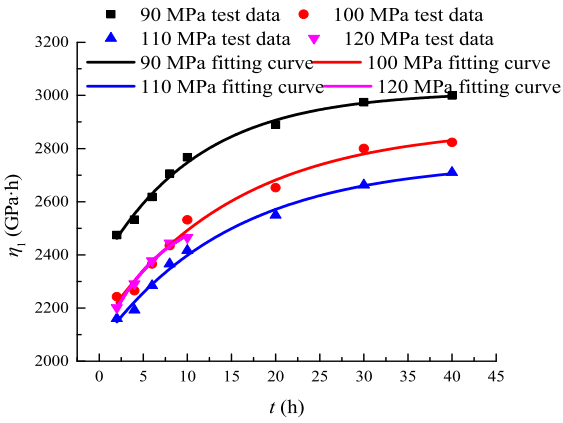

(c) η_1

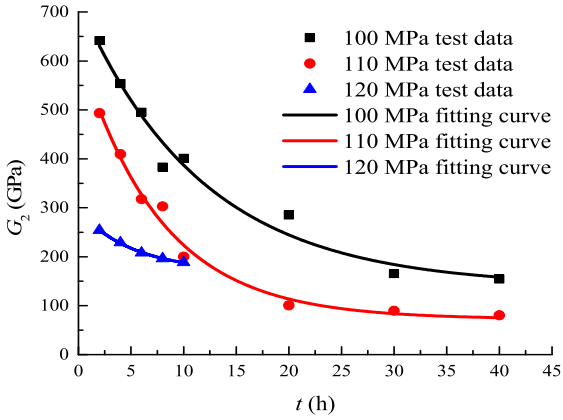

(d) G_2

Fig. 9 (*Continued*)

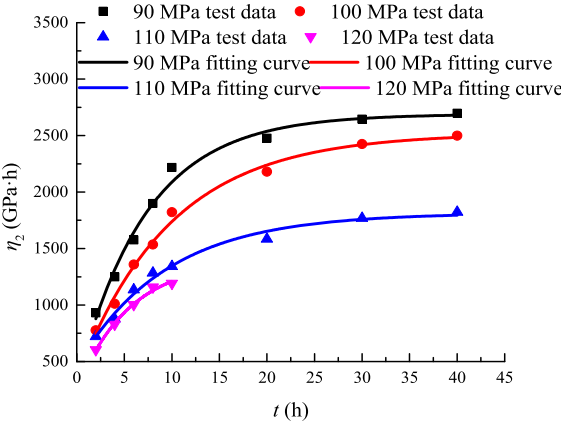

(e) η_2

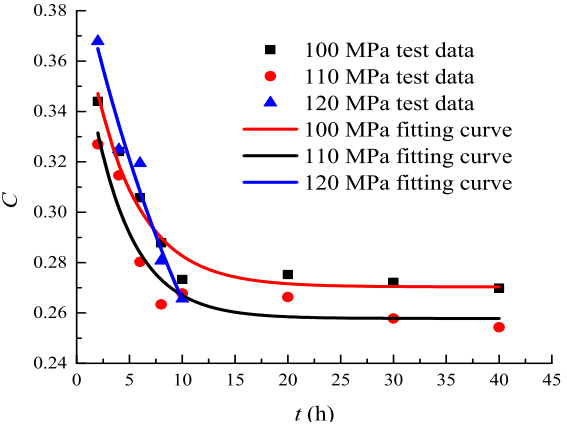

(f) C

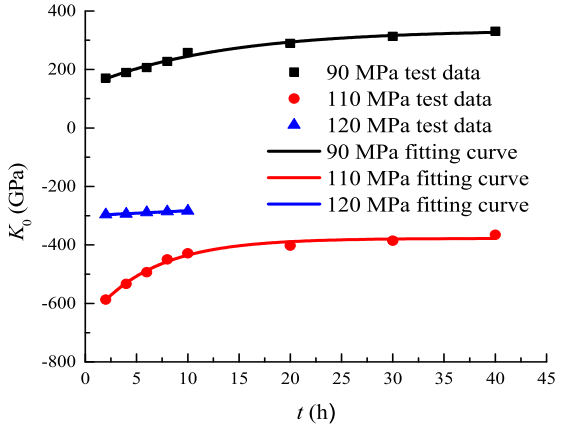

(g) K_0

Fig. 9 (*Continued*)

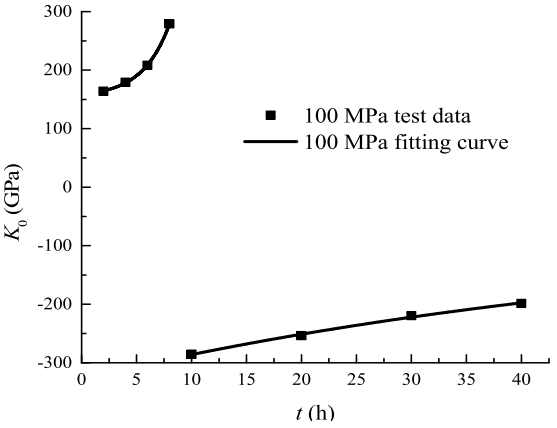

(h) 100 MPa, K_0

Table 3 Fitting parameters (5 MPa)

Parameter	Stress (MPa)	Fitting Parameter		
		a_i	b_i	c_i
K_0 (GPa)	90	−195.779	13.066	336.167
	100 Positive	4.768	−2.448	153.768
	100 Negative	−256.623	56.659	−70.994
	110	−292.366	6.141	−377.583
	120	1429440.000	−852943.503	−1429740.000
G_1 (GPa)	90	8.580	10.047	35.685
	100	12.776	5.737	37.547
	110	15.850	4.503	38.979
	120	−495104.992	−512245.429	495156.213
η_1 (GPa·h)	90	−662.651	11.018	3014.861
	100	−758.120	15.166	2884.578
	110	−692.574	14.995	2753.789
	120	−529.644	6.508	2587.414
η_2 (GPa·h)	90	−2385.193	7.266	2689.933
	100	−2174.407	9.776	2520.257
	110	−1355.167	9.397	1813.926
	120	−1147.548	5.520	1396.955
G_2 (GPa)	100	582.992	11.690	139.262
	110	554.416	7.701	72.422
	120	124.412	5.162	170.095
C	100	0.121	4.36857	0.270
	110	0.124	3.842	0.257
	120	0.267	14.277	0.133

Fig. 10 Contrast curve

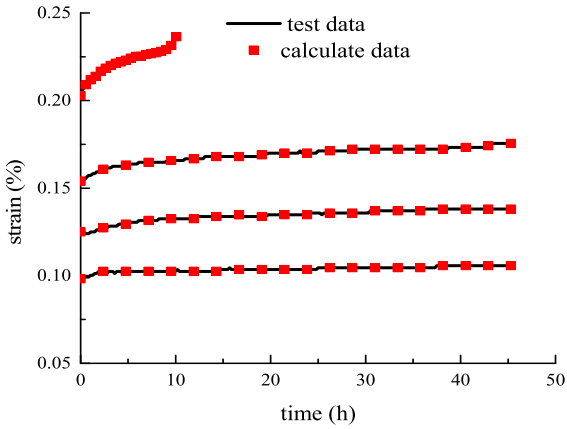

(a)5 MPa

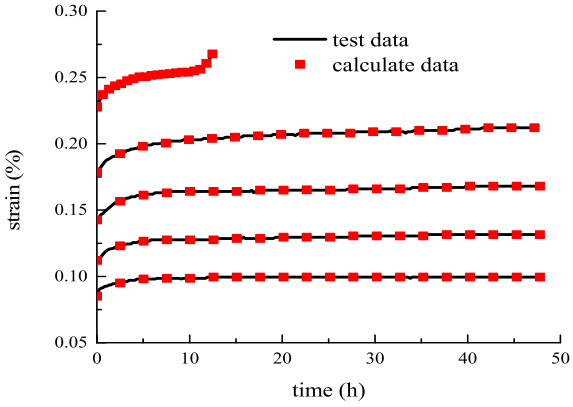

(b)10 MPa

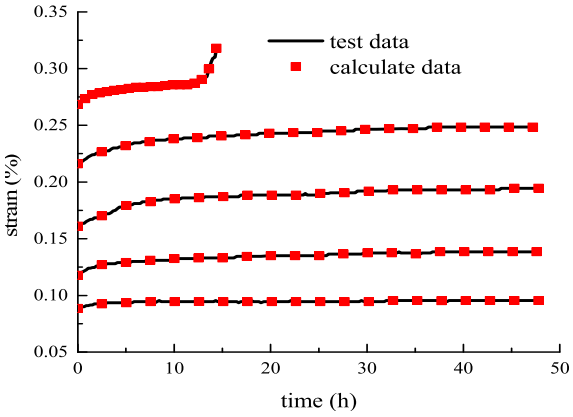

(c)15 MPa

Fig. 10 (*Continued*)

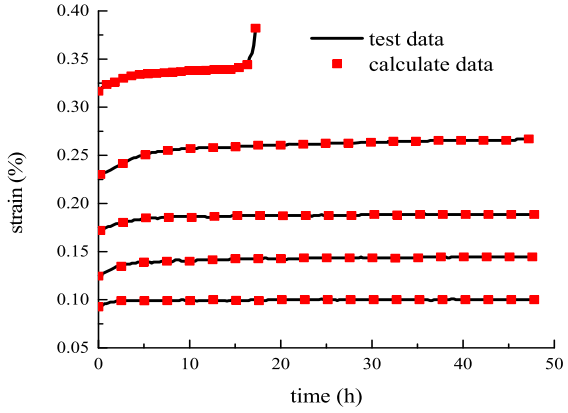

(d)20 MPa

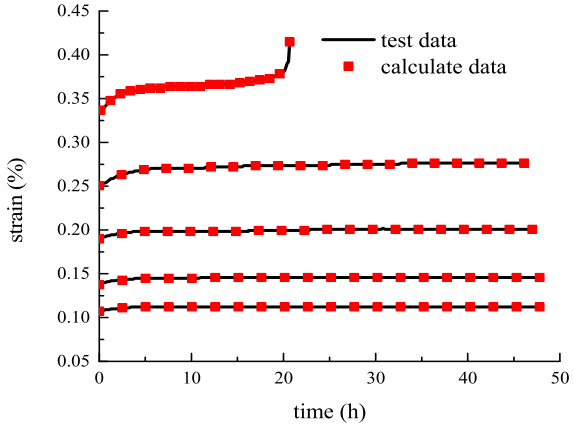

(e)25 MPa

When $\sigma \geq \sigma_s$,

$$\varepsilon_{11} = \frac{\sigma_1 - \sigma_3}{3G_0(\sigma)} + \frac{\sigma_1 + 2\sigma_3}{9K_0(t)} + \frac{\sigma_1 - \sigma_3}{3G_1(t)}\left[1 - \exp\left(-\frac{G_1(t)}{\eta_1(t)}t\right)\right] + \frac{\sigma_1 - \sigma_3}{3\eta_2(t)}t + \frac{\sigma_1 - \sigma_3}{3G_2(t)}\left(\frac{t_F - t}{t_F - t^*}\right)^{-C(t)}. \tag{29}$$

Figure 10 shows the comparison results of the model curve test curve.

As shown in Fig. 10, the curve of the model is consistent with the trend of the test curve, which makes up for the defect that the previous model can not describe the accelerated creep.

To verify whether the method for determining creep parameters applies to other types of rocks, creep curves in other literature (Liu and Zhang 2020b) are selected for comparative analysis, as shown in Fig. 11.

Figure 12 shows the comparison between the literature curve and the model curve. Figure 12 shows that the changing trend of the test curve is consistent with that of the model curve. It is also proved that the creep parameter determination method is correct.

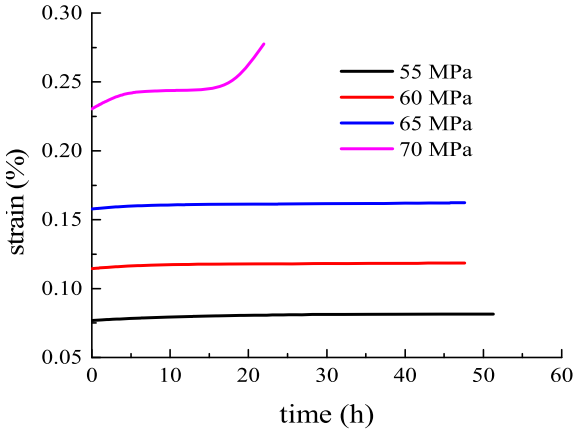

Fig. 11 Axial creep curve of sandstone

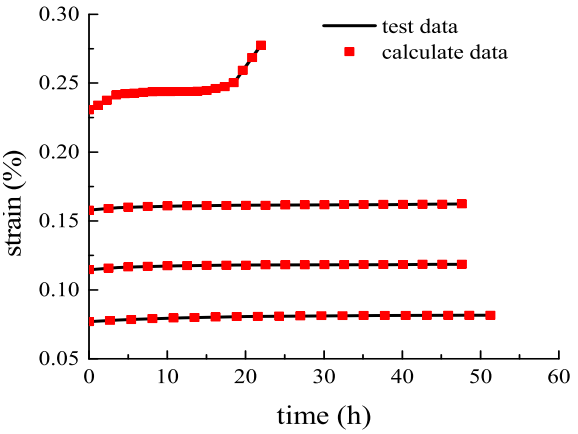

Fig. 12 Comparison between the test and model curves

6 Conclusion

The creep damage evolution equation was established by using the segmentation combination method. A full-process model of nonlinear creep damage was also established. A new method for determining creep parameters is proposed by combining the creep model with creep test data. It can further improve the rheological research theory of rock. The new creep model fits well with the experimental data. It also proves that the method of creep parameter determination is correct. The model also considers the influence of creep parameters on the deterioration of rock structure over time. It is close to the true surrounding rock creep state. A new way of thinking is adopted in constructing rock creep models and practical engineering applications, clarifying the physical meaning of creep parameters.

Acknowledgements The key science and technology special program of Yunnan province (No. 202102AF080001).

Author contributions Wenbo Liu: Conceptualization, data curation, writing-original draft, investigation, and methodology. Hui Zhou: Conceptualization, writing-original draft, writing-review and editing, software, supervision, and methodology. Jian Li: Conceptualization, data curation, methodology, and investigation. Qing Liu:Data processing, document Retrieval Chengwei Zhao:Data processing, document Retrieval Yong Yang:Data processing, document Retrieval

Funding Authors are very grateful for the support of the National Natural Science Foundation of China (51774173).

Declarations

Ethical Statements This material has not been published in whole or in part elsewhere. All authors have been personally and actively involved in substantive work leading to the manuscript and will hold themselves jointly and individually responsible for its content.

Competing interests The authors declare no competing interests.

References

Aditya, S., Chandan, K., Gopi, K.L.: Estimation of creep parameters of rock salt from uniaxial compression tests. Int. J. Rock Mech. Min. Sci. **107**, 243–248 (2018). https://doi.org/10.1016/j.ijrmms.2018.04.037

Andargoli, M.B.E., Shahriar, K., Ramezanzadeh, A.: The analysis of dates obtained from long-term creep tests to determine creep coefficients of rock salt. Bull. Eng. Geol. Environ. **1**, 1–13 (2018). https://doi.org/10.1007/s10064-018-1243-4

Cornet, J.S., Dabrowski, M.: Nonlinear viscoelastic closure of salt cavities. Rock Mech. Rock Eng. **51**(10), 3091–3109 (2018). https://doi.org/10.1007/s00603-018-1506-1

Eslami, A.M.B., Shahriar, K., Ramezanzadeh, A.: The analysis of dates obtained from long-term creep tests to determine creep coefficients of rock salt. Bull. Eng. Geol. Environ. **78**(3), 1617–1629 (2018). https://doi.org/10.1007/s10064-018-1243-4

Hamza, O., Stace, R.: Creep properties of intact and fractured muddy siltstone. Int. J. Rock Mech. Min. Sci. **106**, 109–116 (2018). https://doi.org/10.1016/j.ijrmms.2018.03.006

Hao, T., Wang, D., Huang, R.: A new rock creep model based on variable-order fractional derivatives and continuum damage mechanics. Bull. Eng. Geol. Environ. **77**(1), 375–383 (2017). https://doi.org/10.1007/s10064-016-0992-1

Hou, R., Zhang, K., Tao, J.: A nonlinear creep damage coupled model for rock considering the effect of initial damage. Rock Mech. Rock Eng. **52**(5), 1275–1285 (2018). https://doi.org/10.1007/s00603-018-1626-7

Huang, M., Liu, X.R.: Study on the relationship between parameters of deterioration creep model of rock under different modeling assumptions. Adv. Mater. Res. **243–249**, 2571–2580 (2011). https://doi.org/10.4028/www.scientific.net/AMR.243-249.2571

Jin, J., Cristescu, N.D.: An elastic/viscoplastic model for transient creep of rock salt. Int. J. Plast. **14**(1), 85–107 (1998). https://doi.org/10.1016/S0749-6419(97)00042-9

Jing, W., Yan, Z., Kong, J.: The time-space prediction model of surface settlement for above underground gas storage cavern in salt rock based on Gaussian function. J. Nat. Gas Sci. Eng. **53**, 45–54 (2018). https://doi.org/10.1016/j.jngse.2018.02.024

Li, W.Q., Li, X.D., Bing, H.: Recognition of creep model of layer composite rock mass and its application. J. Cent. South Univ. Technol. **14**(1), 329–331 (2017). https://doi.org/10.1007/s11771-007-0275-x

Liu, Y., Li, Z.D.: Nonlinear variation parameters creep model of rock and parametric inversion. Geotech. Geolog. Eng. **36**(5), 2985–2993 (2018). https://doi.org/10.1007/s10706-018-0517-8

Liu, W.B., Zhang, S.G.: An improved unsteady creep model based on the time-dependent mechanical parameters. Mech. Adv. Mat. Struct. 1–11 (2020a). https://doi.org/10.1080/15376494.2020.1712624

Liu, W.B., Zhang, S.G.: Creep parameter determination and model establishment considering stress and time effects. Geotech. Geolog. Eng. **38**(2), 1509–1520 (2020b). https://doi.org/10.1007/s10706-019-01106-6

Ma, L.J., Liu, X.Y., Qin, F.: A new elasto-viscoplastic damage model combined with the generalized hoek-brown failure criterion for bedded rock salt and its application. Rock Mech. Rock Eng. **46**(1), 53–56 (2013). https://doi.org/10.1007/s00603-012-0256-8

Ma, L., Wang, M., Ning, Z.: A variable-parameter creep damage model incorporating the effects of loading frequency for rock salt and its application in a bedded storage cavern. Rock Mech. Rock Eng. **50**(3), 1–15 (2017). https://doi.org/10.1007/s00603-017-1236-9

Munson, D.E., Weatherby, J.R., Devries, K.L.: Two- and three-dimensional calculations of scaled in situ tests using the M-D model of salt creep. Int. J. Rock Mech. Min. Sci. Geomech. Abstr. **30**(7), 1345–1350 (1993). https://doi.org/10.1016/0148-9062(93)90120-3

Qi, Y.J., Jiang, Q.H., Wang, Z.J.: 3D creep constitutive equation of modified Nishihara model and its parameters identification. Chin. J. Rock Mech. Eng. **31**(2), 347–355 (2012). doi:CNKI:SUN:YSLX.0.2012-02-017.

Riva, F., Agliardi, F., Amitrano, D.: Damage-based time-dependent modeling of paraglacial to postglacial progressive failure of large rock slopes. J. Geophys. Res., Earth Surf. **123**(1), 124–141 (2018). https://doi.org/10.1002/2017JFO04423

Singh, A., Kumar, C., Kannan, L.G.: Estimation of creep parameters of rock salt from uniaxial compression tests. Int. J. Rock Mech. Min. Sci. **107**, 243–248 (2018). https://doi.org/10.1016/j.ijrmms.2018.04.037

Tomanovic, Z.: Rheological model of soft rock creep based on the tests on marl. Mech. Time-Depend. Mater. **10**(2), 135–154 (2016). https://doi.org/10.1007/s11043-006-9005-2

Wang, R., Jiang, Y., Chao, Y.: A nonlinear creep damage model of layered rock under unloading condition. Math. Probl. Eng. **2018**, 1–8 (2018a). https://doi.org/10.1155/2018/8294390

Wang, X., Yin, Y., Wang, J.: A nonstationary parameter model for the sandstone creep tests. Landslides **15**(7), 1377–1389 (2018b). https://doi.org/10.1007/s10346-018-0961-9

Wu, F., Jian, F.L., Wang, J.: An improved Maxwell creep model for rock based on variable-order fractional derivatives. Environ. Earth Sci. **73**(11), 6965–6971 (2015). https://doi.org/10.1007/s12665-015-4137-9

Xu, M., Jin, D., Song, E.: A rheological model to simulate the shear creep behavior of rockfills considering the influence of stress states. Acta Geotech. **13**(4), 1313–1327 (2018a). https://doi.org/10.1007/s11440-018-0716-8

Xu, T., Zhou, G., Heap, M.J., Li, L.C.: The modeling of time-dependent deformation and fracturing of brittle rocks under varying confining and pore pressures. Rock Mech. Rock Eng. **51**(10), 3241–3263 (2018b). https://doi.org/10.1007/s00603-018-1491-4

Yoshida, H., Horii, H.: A micromechanics-based model for creep behavior of rock. Appl. Mech. Rev. **45**(8), 294–303 (1992). https://doi.org/10.1115/1.3119760

Zhou, W., Chang, X.L., Zhou, C.B., Liu, X.H.: Creep analysis of high concrete-faced rockfill dam. Int. J. Numer. Methods Biomed. Eng. **26**(11), 1477–1492 (2010). https://doi.org/10.1002/cnm.1230

Zhou, H.W., Wang, C.P., Han, B.B., Duan, Z.Q.: A creep constitutive model for salt rock based on fractional derivatives. Int. J. Rock Mech. Min. Sci. **48**(1), 116–121 (2011). https://doi.org/10.1016/j.ijrmms.2010.11.004